INTERNATIONAL JOURNAL OF CLIMATOLOGY
*Int. J. Climatol.* **25**: 1437–1454 (2005)
Published online in Wiley InterScience (www.interscience.wiley.com). DOI: 10.1002/joc.1210

# TEMPERATURE RECONSTRUCTIONS AND COMPARISONS WITH INSTRUMENTAL DATA FROM A TREE-RING NETWORK FOR THE EUROPEAN ALPS

DAVID FRANK* and JAN ESPER
*Swiss Federal Research Institute WSL, Birmensdorf, Switzerland*

*Received 21 June 2004*
*Revised 10 April 2005*
*Accepted 18 April 2005*

ABSTRACT

Ring-width and maximum latewood density data from a network of high-elevation sites distributed across the European Alps are used to reconstruct regional temperatures. The network integrates 53 ring-width and 31 density chronologies from stands of four species all located above 1500 m a.s.l. The development and basic climatic response patterns of this network are described elsewhere (Frank and Esper, 2005). The common temperature signal over the study region allowed regional reconstructions to be developed using principal component regression models for average June–August (1600–1988) and April–September (1650–1987) temperatures from ring-width and density records, respectively. Similar climatic histories are derived for both seasons, but with the ring-width and density-based reconstructions seemingly weighted toward carrying more of their variance in the lower and higher frequency domains, respectively. Distinct warm decades are the 1940s, 1860s, 1800s, 1730s, 1660s and the 1610s, and cold decades, the 1910s, 1810s, 1710s, 1700s and the 1690s. Because of the model fitting and the shorter time spans involved, comparisons between the reconstructions with high-elevation instrumental data during the majority of the 1864–1972 calibration period show good agreement. Yet, prior to this period, from which only a few low elevation temperature records are available, a trend divergence between tree-ring and instrumental records is observed. We present evidence that this divergence may be explained by the ring-width data carrying more of an annual rather than warm-season signal in the lower frequency domain. Other factors such as noise, tree-ring standardization, or the more uncertain nature of low-frequency trends in early instrumental records and their homogenization, might help explain this divergence as well. Copyright © 2005 Royal Meteorological Society.

KEY WORDS: dendrochronology; dendroclimatology; temperature reconstruction; Alps; instrumental data; tree-ring width; maximum latewood density

## 1. INTRODUCTION

The use of proxy data plays a significant role in the characterization and assessment of climate variations prior to the instrumental period. Prominent reconstructions of past variability have called upon a combination of tree-ring sites and other proxies (Jones *et al*., 1998; Mann *et al*., 1999; Moberg *et al*., 2005) or specific selections of tree-ring chronologies processed to preserve long-term climate variability (Jacoby and D'Arrigo, 1989; Briffa, 2000; Esper *et al*., 2002; Cook *et al*., 2004; Esper *et al*., 2004). In addition to these large-scale approaches, more detailed studies of regional variations are needed to obtain insight into regionally specific variations and driving factors. In this paper, we consider the climatic signal from a high-elevation temperature sensitive tree-ring network from the European Alps.

The European Alps are influenced by Mediterranean, Atlantic, and Continental Eurasian synoptic systems. In the winter, climate is generally dominated by the North Atlantic Oscillation with some influence from the

* Correspondence to: David Frank, Swiss Federal Research Institute WSL, Birmensdorf, Switzerland; e-mail: frank@wsl.ch

Siberian High. More localized low pressure centers tend to dominate during the summer months. Detailed discussions of climatic influences can be found in Wanner *et al.* (1997).

The early instrumental records available from this area (e.g. Böhm *et al.*, 2001), and proxy records based on historical documentary data (Pfister, 1999) and combinations thereof (Luterbacher *et al.*, 2002; Luterbacher *et al.*, 2004; Casty *et al.*, 2005) have played a vital role in understanding the variability in this region over the past few centuries. Prior tree-ring characterizations of temperature variability have relied upon a selection of maximum latewood density data from this region, which have been analyzed as part of larger European-wide or global networks (e.g. Briffa *et al.*, 1988, 1998, 2002a, 2002b; Schweingruber *et al.*, 1987; Schweingruber and Briffa, 1996), or more local to subregional reconstructions using ring-width data (Serre-Bachet *et al.*, 1991; Nicolussi and Schiessling, 2001; Wilson and Topham, 2004; Büntgen *et al.*, 2005). Herein, we consider large networks of both ring-width and density data from high-elevation sites across the central and western Alps to develop June–August (JJA) and April–September (A–S) mean temperature reconstructions. These reconstructions display similarities reflecting the common seasonal signal, yet simultaneously, show differences, which we relate to the particular way the ring-width and maximum latewood density parameters record climatic variation.

The Alps have unique characteristics for dendroclimatological studies. In contrast to most areas of the world, instrumental records in this region span over two centuries. This has the advantage of allowing calibration and independent comparisons between tree-ring and instrumental data over rather long periods of time (Böhm *et al.*, 2001; Luterbacher *et al.*, 2004). On the other side, the Alps are heavily impacted by human and animal activities, resulting in relatively few undisturbed forests.

This paper contains six sections. In the following section, the tree-ring and instrumental data are introduced. The third section contains a reconstruction of JJA temperatures derived from the ring-width data. The fourth section presents reconstructions of A–S temperatures derived from the density data using two different methods, with the second being less conventional but seemingly more successful. A discussion of the reconstructions, derived Alpine temperature histories and comparisons with instrumental data, is given in the fifth section. A summary is given in Section 6.

## 2. DATA

### *2.1. Tree-ring data*

Tree-ring data from a network of 53 sites above 1500 m a.s.l. from the Central and Western Alps are used (Figure 1). Maximum latewood density data are available for 31 of these sites. *Picea abies, Abies alba, Larix decidua*, and *Pinus cembra* (herein, abbreviated as PCAB, ABAL, LADE and PICE) are the four species included in the network; the majority of sites are PCAB. Ring-width series were standardized by using an adaptive power transform to stabilize the variance (Cook and Peters, 1997), and then residuals from a spline with a 300-year frequency-response cutoff were taken (Cook and Peters, 1981) to remove the age trend. Density series were detrended by taking residuals from linear fits of any slope. Chronologies were averaged on a site-by-site basis using a robust mean (Cook, 1985), adjusted for changes in variance related to changes in sample size and interseries correlation (Osborn *et al.*, 1997), and truncated at a minimum sample size of five series. These detrending methods should be sufficient to remove age-related trends, without removing significant climate information on annual to multi-decadal timescales. Centennial scale climatic trends, if they exist, will be removed by this detrending (Cook *et al.*, 1995). After truncation, median chronology lengths are 193 and 171 years for ring-width and density, respectively. A more detailed analysis of these sites, inter-correlations, climate responses, and regional details are given in Frank and Esper (2005). The network ring-width data primarily reflect JJA, and the density data, A–S and seasonal temperatures (Frank and Esper, 2005).

### *2.2. Instrumental data*

Prior to use, instrumental data had been subjected to homogeneity tests and adjustments, spatial and temporal analyses and gridded on a $1 \times 1$ degree network (Auer *et al.*, 2000; Böhm *et al.*, 2001). This dataset contains

 

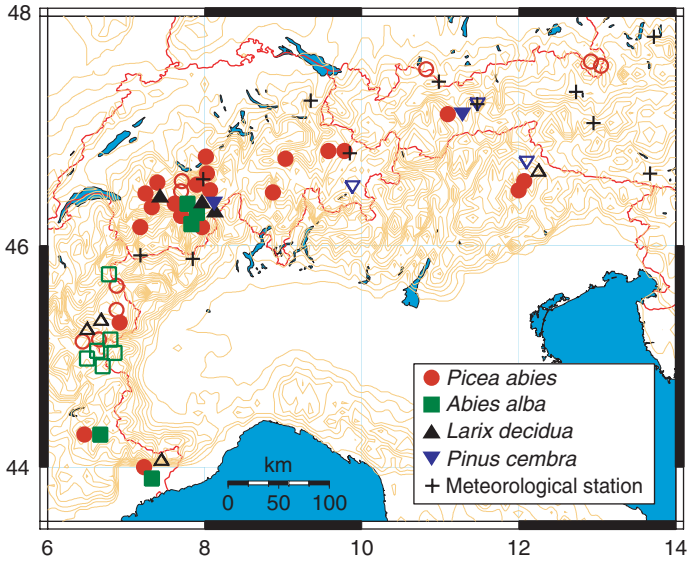


Figure 1. Map showing the locations of the 53 tree-ring sites included in the network. Sites are differentiated by species and whether ring-width and maximum latewood density parameters were both available for a site (filled symbol) or only ring-width (empty symbol). The locations of the 11 meteorological stations used to make the high-elevation gridded data (Böhm *et al*., 2001) are also shown. All tree-ring sites and meteorological stations are above 1500 m a.s.l. This figure is available in colour online at www.interscience.wiley.com/ijoc

a high-elevation grid of 16 points, coinciding with the core of the Alpine arc, derived from 11 stations all located above 1500 m a.s.l. The common period for these 16 grid points is 1864–1998. Additionally, a low elevation grid covering a much wider area is also available. Early instrumental data are available from urban stations, such as Geneva and Milan, and set the start date for the earliest gridded data in the Böhm *et al*. (2001) data set at 1760. Stations used in the low-elevation grid are different from those used in the high-elevation grid. See Böhm *et al*. (2001) for details. Data from a single low elevation grid point (47 °N, 9 °E) from about the center of the network are used for additional verification and comparisons.

## 3. RECONSTRUCTION METHODS

Aside from some regional gradients, comparison of tree-ring and instrumental data demonstrated a significant homogeneity of high-elevation temperature data across the Alps. For example, correlations between seasonal means from high-elevation instrumental stations tend to be above 0.8. (Böhm *et al*., 2001; Frank and Esper, 2005). Differences in the climatic regimes are likely within the range of unexplained variance of tree-ring reconstructions, so averages of the 16 point, high-elevation grid, derived from 11 stations all located above 1500 m a.s.l., are used as the reconstruction target. The high-elevation grid data were averaged over the 1864–1998 common period into two seasons; JJA as a target for ring-width, and A–S for density.

To take advantage of the full spatial and temporal range covered by the tree-ring network, and considering the fact that the number of available chronologies decreases back in time, we chose to develop nested principal component regression models (as in Cook *et al*., 2002, 2003). This decision follows the premise that greater reconstruction skill is obtained when more tree-ring series are available as predictors. In this technique, individually calibrated models using all available predictors within a given time period are developed and are then spliced together so that a near-maximum number of predictors is used to estimate temperatures back in time.

From the climate response of the individual sites, it is apparent that not all tree-ring records are ideal predictors (Frank and Esper, 2005). Chronologies in years $t$ and $t+1$ (corresponding to the rings formed

 

during the instrumental target season and the following year) were considered as predictors, but only those that passed a two-tailed test of significance at the $p < 0.1$ level were allowed to enter the principal component regression analysis. Principal components analysis (PCA) is performed on all retained predictors, and the first $n$ eigenvectors, following the Kaiser-Guttman rule, that had eigenvalues $>1$ were then retained for the multiple regression. The $n$ eigenvectors were serially entered into multiple regression models in the order of their correlation with the calibration data. The final model was selected based on the minima in the Akaike information criteria, which balances explained variance and degrees of freedom by using a penalty term that increases with the number of predictors used for a model (Akaike, 1974).

The primary period of instrumental-proxy overlap (1864–1972) was split in half (1864–1918, 1919–1972) to allow for calibration/verification tests. To statistically assess the reconstructions, the Sign and Product Mean tests, and the Coefficient of efficiency (CE) and Reduction of Error (RE) statistics, are used. The RE statistic can range from 1 to minus infinity and compares whether reconstructed values possess more skill than the mean of the calibration period, with positive values indicative of this skill. The CE is similar to the RE but compares estimates with the mean of the verification period, making this a rigorous statistic that is difficult to pass, particularly when there are low-frequency variations and substantial differences in the means of the calibration and verification periods. See Cook *et al.* (1994) for more details on these statistics. Final models were calibrated over the full 1864–1972 period.

Reconstruction uncertainty is defined by +/− the root mean square error (RMSE) between the smoothed reconstructed and instrumental data. Maximum overlap between the nests and the 1760–1863 and the 1973–1989 (non-calibration) instrumental data were used to calculate the RMSE (except for the 1850–1973 nests for which the 1850–1972 instrumental data were used). Discontinuities between nest uncertainties were smoothed with a 31-year Gaussian filter. These error estimates are primarily derived from data outside the calibration interval, and as calculated are similar to the RMSE of validation (Weisberg, 1985; Meko *et al.*, 2001).

To determine the relative influence of the chronologies on the reconstruction, in terms of species and geographical position, the absolute values of the standardized regression coefficients (beta weights), which represent the loadings of the predictors in the principal components regression, were taken. These were summed for a site in the few cases where both years $t$ and $t + 1$ entered the regression, and expressed as a percent of the absolute sum of the beta weights. Results are plotted on maps.

## 4. TEMPERATURE RECONSTRUCTIONS

### *4.1. JJA reconstruction*

For the ring-width-based JJA temperature reconstruction, seven time intervals for PCA were defined, with the main interval spanning 1850–1973. The other intervals increase in length in 50-year time steps back to 1600. An additional 1850–1990 period was defined to allow tree-ring data to be transferred into the recent decades, where again fewer chronologies exist, as many of the sites were sampled in the 1970s.

Calibrating and verifying the data over both the 1919–1972 and 1864–1918 time periods resulted in 14 models. Results are summarized in Appendix Ia. The explained variance of the regression in the calibration period ranges from 31 to 68%, with smaller values occurring as fewer and fewer predictors enter the model back in time. Explained variance in the verification periods ranges from 25 to 43%. All of the models have values greater than zero for the RE statistic, indicating the models have predictive skill in comparison to the mean of the calibration period. Most of the models have negative values for CE statistic, however, indicating potential limitations in the low-frequency component of these models, which will be addressed later. Values for the Sign and Products Mean tests are generally significant at or above the 90% level. In general, these calibration and verification results suggest that these models have predictive skill and can be merged into a composite reconstruction.

Data from the seven PC windows were then calibrated over the full 1864–1972 period for the final reconstruction. The resulting models were then scaled to the mean and variance of the 1864–1972 instrumental data. The seven models and their calibration statistics are shown in Figure 2A and Appendix IIA. Like the

 

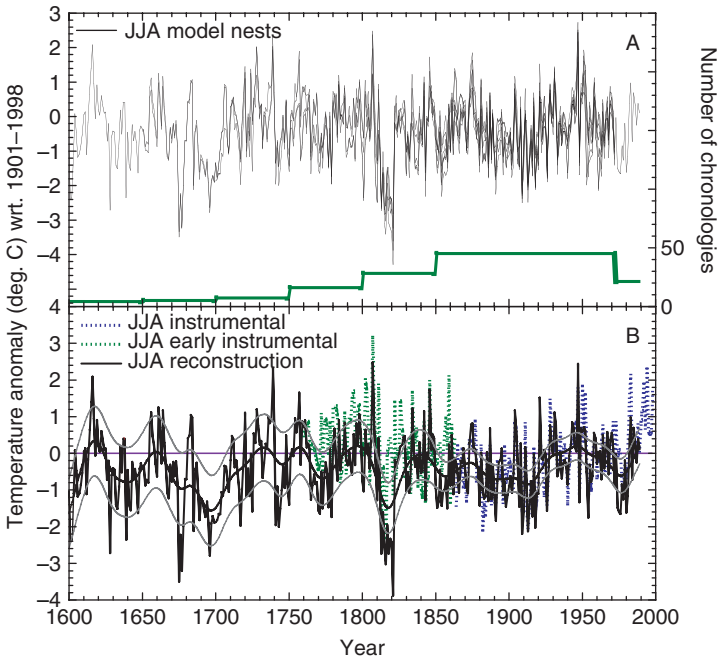


Figure 2. JJA temperature models derived over the full 1864–1972 calibration period. Temperatures are anomalies with respect to the 1901–1998 average. (A) The seven different ring-width nests and the available number of chronologies in each time period for PC regression. The 1850–1973 period serves as the main nest and is common to all subnests. The individual models were spliced together to form the final JJA temperature reconstruction shown in (B), along with high elevation JJA temperature data (1864–1998) and early instrumental data (1760–1863). The smoothed reconstruction and +/− RMSE limits for this smoothing are shown. See text for details. This figure is available in colour online at www.interscience.wiley.com/ijoc

subintervals tested above, the variance explained in the calibration period increases with the number of predictors and ranges from 28 to 62%. For every time period, most of the available chronologies were used in the calculation of the principal components. For example, 45 chronologies met the time requirements for the 1850–1973 model. Of the total possible 90 $t$ and $t + 1$ predictors, 50 passed the correlation screening (33 for year $t$ and 17 for year $t + 1$) with 39 of the 45 chronologies represented.

The individual subset models show similar patterns (Figure 2A) in both extreme values and multi-decadal fluctuations. During the 1850–1972 period, the seven models have an average inter-correlation of 0.79, with a minimum correlation of 0.55 between the 1850–1990 and 1600–1973 models that had 21 and 4 predictor chronologies available, respectively. For additional verification, these models (except for the 1850–1990 nest; see Appendix II legend) were correlated with average JJA temperatures from a single, low-elevation grid point (47 °N, 9 °E) near the center of the network. Negative RE and CE statistics are indicative of the lower frequency divergence between the instrumental data and proxy reconstruction. This will be addressed in Section 5.3. Variance explained with the independent and primarily early, instrumental data range from 14 to 49%, typically with diminishing values as the number of predictor chronologies decrease (Appendix IIA). These results are somewhat unexpected if considering only the coherent picture of the individual models shown in Figure 2A, but demonstrate the value in using a greater number of tree-ring chronologies.

Beta weight results for the 1850–1973 nest are shown in Figure 3, along with the locations of those chronologies that did not enter the PCA because of their length or did not pass the initial screening. Weights are distributed geographically and species-wise across the network, with the median relative loading of 1.9%. ABAL tends to have lower loadings likely due to the more unique climate response of this species, and its occurrence in the more Mediterranean-influenced region (Frank and Esper, 2005). LADE and PICE tend to have higher loadings with average values of 4.9 and 3.2%, respectively. All of the beta weights for year $t$ are positive except for four PCAB and two ABAL sites. On the other hand, all beta weights of the PCAB

 

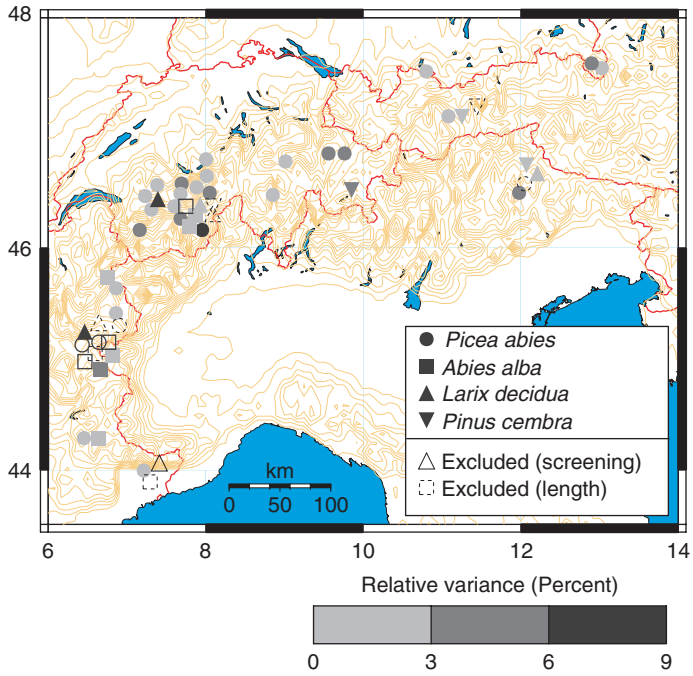


Figure 3. The absolute values of the beta loadings (expressed as a percent of the total absolute beta weight sum) for all chronologies used in the JJA 1850–1973 nest. The beta weights represent the regression coefficients transferred back in terms of the initial predictors (the chronologies). For the chronologies with predictors in years $t$ and $t+1$, beta weights were summed. The distribution of beta weights across species and space show that information in the reconstruction comes from across the entire network. This figure is available in colour online at www.interscience.wiley.com/ijoc

and ABAL chronologies with predictors in year $t+1$ are negative, consistent with their climate response tendency for negative correlations with prior summer growth. The majority of these chronologies are located in southwestern Switzerland.

The final JJA temperature reconstruction is derived from splicing the individual models together, so that the 1850–1973 model is used over its full time span and then the additional models successively attached. The JJA temperature reconstruction, with the calibration data and the early additional verification data, is shown in Figure 2B.

### *4.2. A–S reconstruction*

The same reconstruction methods applied to the ring-width data were employed on the density data. Due to the lower number and shorter average length of density chronologies, four time nests were defined, with the 1830–1973 period serving as the main nest. Two 50-year extensions to this nest and an additional 1830–1988 nest were also computed (Appendix IB). Calibration and verification tests were again performed on the 1864–1918 and 1919–1972 time periods. Explained variance in the calibration period ranges from 33 to 54%, and almost identically from 32 to 53% in the verification period. RE values, except for one, are all positive, and CE values are again less than zero. The Sign test for the early verification period was not passed at the 90% level, but all late verification period tests were passed at the 95% level. Product Mean tests were all passed above the 99% levels. In general, the different nested models display a consistent picture and are statistically shown to have predictive skill. The final models were calibrated over the full 1864–1972 period, scaled to the instrumental temperature data over the 1864–1972 interval, and spliced together (Figure 4A and Appendix IIB).

In all of the models, all available chronologies passed the correlation screening at lag 0, but only a few passed at lag 1. Even though the number of available chronologies ranges from 4 to 19, these models are

 

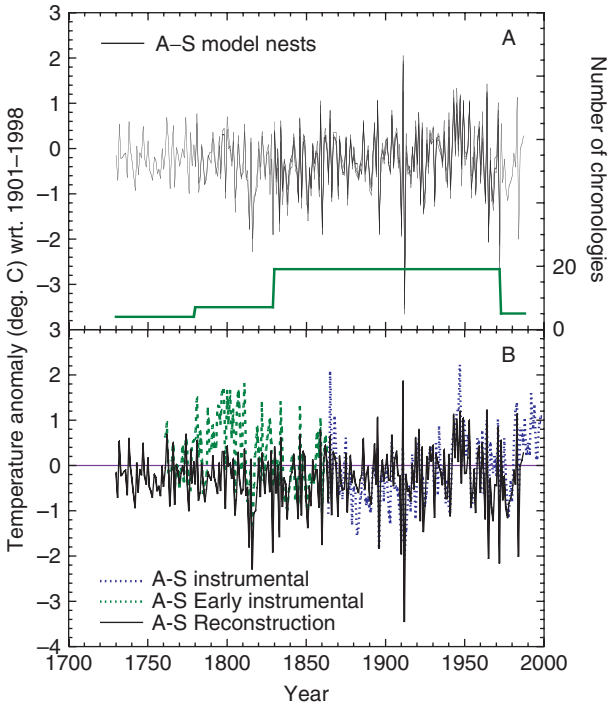


Figure 4. A–S temperature models derived over the full 1864–1972 calibration period. Temperatures are anomalies with respect to the 1901–1998 average. (A) The four different density nests and the available number of chronologies available in each time period for PC regression. The 1830–1973 period serves as the main nest and is common to all subnests. The individual models were spliced together to form the final A–S temperature reconstruction shown in (B), along with high elevation A–S temperature data (1864–1998) and early instrumental data (1760–1863). This figure is available in colour online at www.interscience.wiley.com/ijoc

nearly identical as seen graphically (Figure 4) and statistically (Appendix IIB), with the lowest correlation of 0.94 between the 1730–1973 and 1830–1988 nests over their common period. Variance explained during the calibration ranges from 38 to 43%. The extra verification statistics for the full model are generally favorable, aside from the negative CE values and less significant Sign statistics during the earlier period. Explained variance with the verification data is fairly consistent and ranges from 43 to 57%. We attribute the similarity of these models to be a result of the high common signal across the density network (Frank and Esper, 2005).

This similarity had the further effect that in all four models only the first and second eigenvectors had eigenvalues $>1$, both of which were always used in modeling based on the Akaike criteria. For example, the first eigenvector in the 1830–1973 nest contains 63% of the variance, representing a sizeable fraction of the common network signal. The common signal across the sites, the specific methods for temperature reconstruction and also the length of this reconstruction provide opportunities for trying other methods for improving the A–S temperature reconstruction, which will be discussed below.

The relative contribution of the sites to the 1830–1973 model, calculated as a percent of the (summed) absolute values of the beta weights, is shown in Figure 5. Of the 31 sites with density data, 19 met the length requirements for this model. This length exclusion only left a single ABAL chronology from the southwestern portion of the network. Further, no PICE and only one LADE chronology met the length thresholds. Hence, the resulting reconstruction acquires most of its information from PCAB chronologies in the northern and eastern portions of the network.

Of the chronologies included, variance is broadly distributed throughout the network (Figure 5). The median percent contribution for the 19 sites is 4.8%, with the single ABAL and LADE sites having respective loadings of 1.4 and 10.6%, representing the minimum and maximum loadings of all sites. High contributions also come from the four eastern PCAB sites, but with many of the PCAB sites in southwestern Switzerland strongly

 

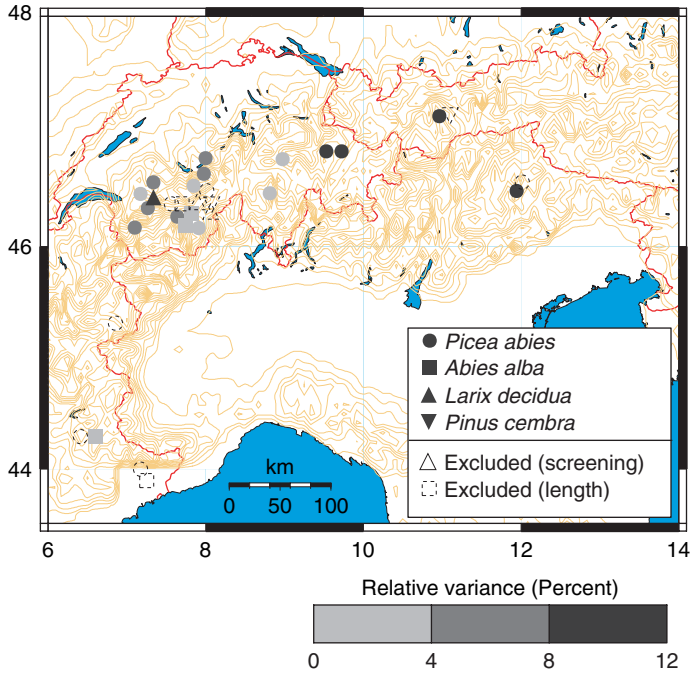


Figure 5. The absolute values of the beta loadings (expressed as a percent of the total absolute beta weight sum) for all chronologies used in the A–S 1830–1973 nest. The beta weights represent the regression coefficients transferred back in terms of the initial predictors (the chronologies). For the chronologies with predictors in years $t$ and $t + 1$, beta weights were summed. This figure is available in colour online at www.interscience.wiley.com/ijoc

contributing, as well. Three chronologies entered the PC modeling in the year $t + 1$; all were PCAB sites from southern Switzerland. Beta values for these three predictors are negative, whereas all lag 0 beta values are positive.

The merged A–S density reconstruction is shown in Figure 4B, along with the calibration data and early instrumental verification data.

### *4.3. A–S reconstruction – take II*

The high common signal seen within the density network, its consequences on the principal component regression procedure and truncating density chronologies at a minimum of five series on a site-by-site basis allow potential opportunities to improve the model and length of temperature reconstruction. To explore this possibility, we attempted the same basic modeling procedure as outlined above, except this time using the individual detrended density series, rather than the mean site chronologies, as predictors. The conceptual basis for this procedure is the high common signal found across the density sites. This has the effect of lengthening the potential reconstruction period, as individual long-lived trees from single sites would remain as predictors, as well as increasing the number of potential predictors at all stages of the modeling. This procedure is a simplification of a method devised and described by Meko (1997), where individually detrended tree-ring data and their associated climatic data from individual meteorological stations are subjected to principal components regression. Peters *et al*. (1981) similarly describe additional information that may be derived by analysis of within-site principal components.

Six PC nest intervals were defined with the first covering the 1850–1973 window, and subsequent nests stepping back every 50 years until the 1650–1973 common period. Again, a modern nest from 1850 to 1988 was defined. High values for explained variance (as high as 94%, Appendix IC) during the calibration are a result of the large number of predictors available, and it is likely that overfitting of this model during the calibration period occurs. However, any overfitting in the calibration period does not seem to be a serious

 

problem when considering the corresponding verification statistics. Most of the models have significant values for the Sign and Product Mean tests. Variance explained during the verification period ranges from 21 to 56%, RE values are all positive and in contrast to the models presented above, CE statistics are positive in 8 out of 12 cases. Although, still primarily a statistical test in higher frequency agreement, the generally positive CE values suggest that these models perform reasonably well in capturing the lower frequency instrumental changes (as measured by the mean) from the calibration to verification periods (Appendix IC).

As done above, for the final reconstruction, these models were calibrated and scaled over the full 1864–1972 period (Appendix IIC, Figure 6A). In the 1850–1973 model, of the 341 series that met the length requirements, 307 year-$t$ predictors passed the initial screening. All but one of these 307 predictors had positive correlations (averaging 0.42) with the A–S instrumental data. In contrast, 82 of the 89 year $t + 1$ predictors that passed screening had negative correlations with the instrumental data. Percent loadings, again as measured by the (summed) absolute value of beta weights, show incorporation of information from across the network, with a median value of the 333 series of 0.24%.

The individual models are again fairly similar, although have substantially greater differences than the site-wise density reconstruction, which we attribute to the large ranges of predictors available for the different model periods. The average correlation between these models is 0.85 with the minimum correlation of 0.71 occurring between the 1650–1973 and 1850–1973 models. Again, highly significant explained variances, ranging from 37 to 65% of the extra verification data are obtained for these models. The extra verification statistics are favorable, with only negative CE values in the earliest two nests, again pointing toward low-frequency divergence between the reconstruction and early instrumental data.

As also indicated by the verification statistics, these models seem to retain more low-frequency variation than the site-wise density models. The final individual-series-based reconstruction is shown in Figure 6B and in Figure 6C, where it is compared with the site-wise density reconstruction from above. Even though the approach used to make this individual-series-based reconstruction is non-conventional, the verification statistics, greater length, yet similarities to the more conventional approach, suggest it is a better and more useful estimate of A–S temperatures, and hence we will use this result as the A–temperature reconstruction.

## 5. DISCUSSION

### *5.1. Western and Central Alpine temperature history*

The JJA reconstruction shows relatively cool conditions during much of the seventeenth and early eighteenth centuries, relative warmth from the 1720s until about 1810, followed by an exceptionally cold period from about 1810 until 1821 after which temperatures rapidly rebound, but remain relatively cool until the 1940s. The highest value of the entire reconstruction is about 2.5 °C warmer than the twentieth-century mean for the summer of 1807. This is also the warmest summer in the 47 °N, 9 °E grid point during the 1760–1998 period (Böhm *et al*., 2001). The lowest reconstructed value is in the year 1821, with a reconstructed temperature departure of nearly 4 °C colder than the twentieth-century mean. This year comes at the end of an extremely cold decade, coinciding with the Dalton minimum in solar activity and following substantial volcanic activity including the 1815 eruption of Tambora (Crowley, 2000).

The density based A–S reconstruction shows similar characteristics to the JJA reconstruction. One of the more notable differences is that the cooler conditions from the early 1800s until the 1940s are interrupted by warmer conditions in around the 1860s. The warmest (1947) and coldest (1912) A–S seasons reconstructed both occur during the calibration period. These years coincide with the warmest and coldest A–S seasons in the full range of the 1760–1998 instrumental data. In general, there is good agreement between the JJA and A–S reconstructions in these decadal comparisons. Distinct warm decades are: the 1940s, 1860s, 1800s, 1730s, 1660s and 1610s; distinct cold decades are the 1910s, 1810s, 1710s, 1700s and 1690s (Table I).

The density record contains overlap with the data used by Briffa *et al*. (1988) to reconstruct European A–S temperatures from 1750, and similarly with those in the Southern Europe (SEUR) reconstruction of Briffa *et al*. (2001) where an age-related standardization method (Age Banding) was introduced to preserve long-term variability. These reconstructions represent a much larger area, spanning well beyond the Alps. Comparison

 

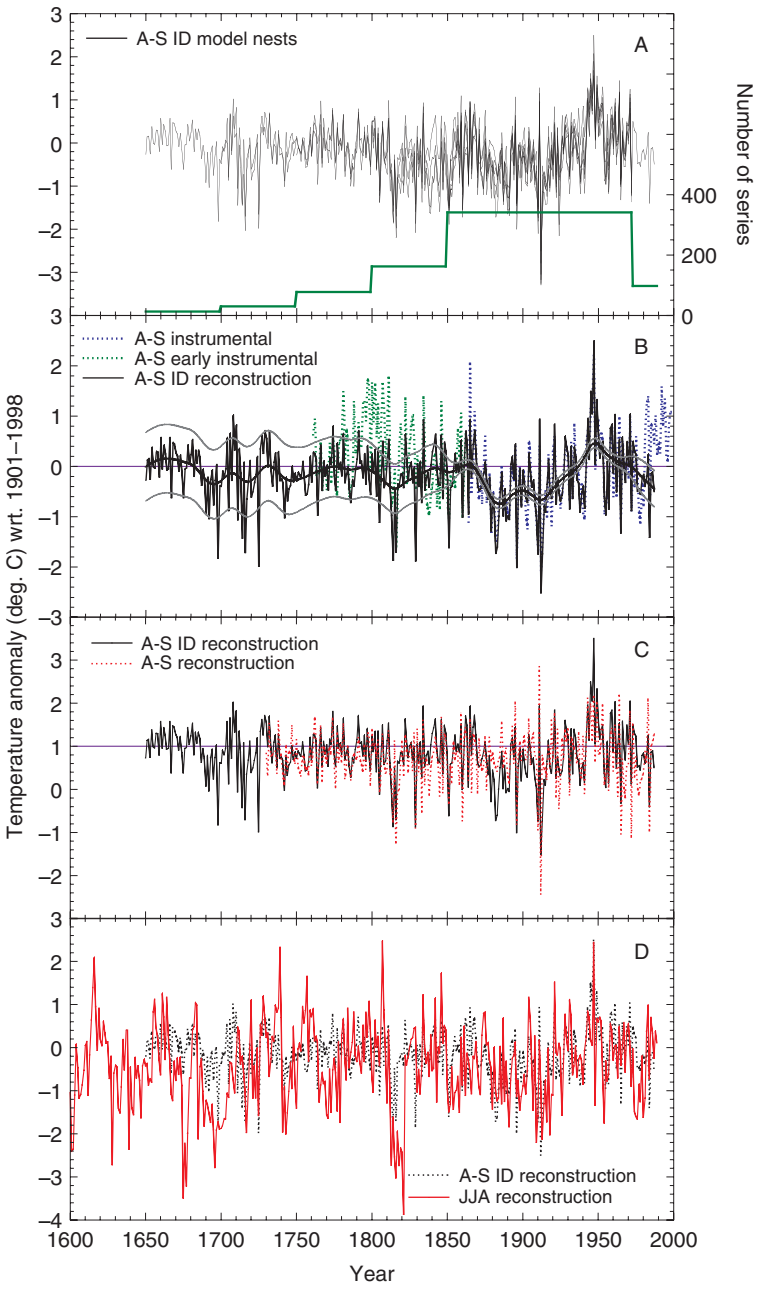


Figure 6. A–S temperature models derived over the full 1864–1972 calibration period. Temperatures are anomalies with respect to the 1901–1998 average. In contrast to the other models presented, these models are based on principal components from the individual (detrended) measurement series. (A) The six different density nests and the available number of series in each time period for PC regression. The 1850–1973 period serves as the main nest and is common to all subnests. The individual models were spliced together to form the final individual series A–S temperature reconstruction shown in (B), along with high elevation A–S temperature data (1864–1998) and early instrumental data (1760–1863). The smoothed reconstruction and +/− RMSE limits for this smoothing are shown. See text for details. A comparison of this individual series reconstruction and those based on chronologies is shown in (C). Due to the better verification statistics, similar characteristics to the chronology-based A–S reconstruction and greater length, this individual series A–S reconstruction is retained as the best and most useful estimate of A–S temperatures. It is compared with the JJA reconstruction in (D). This figure is available in colour online at www.interscience.wiley.com/ijoc

 

Table I. Warmest and coldest decades for JJA & A–S reconstructions

| Century | Warmest decade | | Coldest decade | |
|---|---|---|---|---|
| | JJA | A–S | JJA | A–S |
| 20th | 1940 | 1940 | 1910 | 1910 |
| 19th | 1800 | 1860 | 1810 | 1810 |
| 18th | 1730 | 1730 | 1700 | 1710 |
| 17th | 1610 | 1660 | 1690 | 1690 |

of the density reconstruction with the 45 °N, 10 °E gridpoint of the Briffa *et al*. (1988) reconstruction reveals fairly similar patterns of variability, with correlations in the pre-calibration period of overlap (1750–1863) of 0.29. The correlation with the SEUR record over the 1750–1863 period is 0.53 and 0.31 when including the early data from 1650 to 1863. This latter reduction is additionally related to a substantial trend difference noted with the early period of the SEUR reconstruction, prior to about 1700, where the Age Band detrended SEUR record and the conventionally detrended record presented in Briffa *et al*. (2001) are shown to diverge.

The reconstructions developed by Luterbacher *et al*. (2004) and particularly that of Casty *et al*. (in press) span a similar region. These multi-proxy reconstructions used early instrumental data and hence are quite similar to the early verification data shown herein. More details and comparisons over longer time periods can be found in Büntgen *et al*. (2005).

### *5.2. Statistical characteristics of the reconstructions*

The ring-width based JJA and the individual series density based A–S reconstructions show similar histories in terms of above- and below-average temperatures, although are of quite different characteristics (Figure 6D). The JJA and A–S instrumental series have an average correlation of 0.76 during the 1864–1998 period and standard deviations of 0.90 and 0.80 °C, respectively. The correlation between the two reconstructions during their common period outside of the calibration interval (1650–1863) is 0.28. After filtering with a 10-year spline, these series correlate at 0.45 and 0.17 for the low- and high-frequency components, respectively. A notable feature of the A–S reconstruction is the difference in variability throughout the record, with particularly little variation between the early eighteenth and nineteenth centuries. The standard deviation for the pre-calibration period is 0.49 °C, while that for the calibration period (1864–1972) is 0.77 °C. In comparison, standard deviations for the ring-width reconstruction are 1.03 °C and 0.82 °C for the pre-calibration (1600–1863) and calibration (1863–1972) periods, respectively, indicating a slightly more stable variance through time. Lag 1 autocorrelations for the instrumental data are 0.35 and 0.26 for JJA and A–S, respectively, while those for the pre-calibration period of the reconstructions are 0.54 and 0.03.

It is likely that many of the statistical differences between the JJA and A–S reconstructions result from the different characteristics and strengths of the ring-width and density parameters. The density parameter shows a stronger common signal across the network, rather independent of species and site ecology, and yields stronger calibration and verification statistics with climate data. However, comparisons of high- and low-pass filtered ring-width and density responses to climate show that the density series contain a greater fraction of their signal in the high-frequency domain, whereas the ring-width series contain a greater fraction of their signal in the lower frequency domains (Frank and Esper, 2005). These characteristics seem to apply to the subsequent reconstructions as well. The reduced standard deviations and the essentially zero lag 1 autocorrelation in the reconstructed period perhaps suggest some limitations to the density reconstruction beyond inter-annual to decadal wavelengths. Such potential limitations of the density data could be masked in the calibration and verification results, as essentially all statistical tests are controlled by the high frequency domain skill. However, conversely, the ring-width data have more autocorrelation, likely enhanced by biological feedbacks, and consequently limited to optimally reconstruct JJA temperatures with their lower lag 1 autocorrelations, for example.

 

*5.3. Lower frequency patterns in the reconstructions*

The extended instrumental records from stations surrounding the Alps provide the ability to compare the relative performance of tree-ring based reconstructions over lengthy time periods. In addition to the already relatively long high-elevation instrumental data back to 1864, exceptionally long, but low elevation station data (back to 1760) can be used to further assess the reconstruction skill and, in particular, the lower frequency components.

Low-frequency discrepancies between the reconstructions and the early instrumental data are evident in Figures 2B, 4B and 6B. These discrepancies are particularly visible in the late eighteenth and early nineteenth centuries. Anomalies calculated between the reconstructed and instrumental data smoothed with an 11-year running average (Figure 7) show these differences more explicitly. The ring-width-based reconstruction substantially underestimates temperatures during the most of the overlap period with early instrumental data, with substantially lower values during the late 1700s and maximal divergence during the temperature minima around 1815. The exceptionally cold temperatures reconstructed in the early nineteenth century, are found in many regional to global scale temperature reconstructions (e.g. Briffa *et al.*, 2002a). Cold temperatures, but of a lesser severity, are also recorded in the early instrumental data and reconstructed in the A–S density based reconstruction. It is not certain, if, and to what extent, non-linearities or biological feedbacks have amplified these cool conditions in the ring-width response. The JJA reconstruction also shows another period with lower values centered around the 1850s. The density-based reconstruction shows maximal divergence during the warm period centered at about 1800.

Divergence between the tree-ring and instrumental data are perhaps most basically explored by trying to understand the loss of (low frequency) climatic information during detrending. The use of rather conservative, relative to the segment length and time spans involved, 300-year splines seek to minimize this loss, but this loss is inherent (Cook *et al.*, 1995) when not using age-related detrending approaches such as, regional curve standardization (RCS; Briffa *et al.*, 1992). This dataset does not meet sample distribution and sample size prerequisites for the robust application of RCS, so analysis of the splines used in detrending (sensu Esper *et al.*, 2003) was undertaken, but did not clearly reveal systematic evidence of lost information.

The divergence between the tree-ring and instrumental data can potentially be explained within the context of the seasonal response of the trees. Indications that trees transport information related more to annual temperature variability, particularly in the lower frequency domain, due to biological and physical processes and feedbacks such as needle growth and retention in most conifers, photosynthesis occurring outside the growing season, soil temperatures and their effect on root activities (D'Arrigo *et al.*,

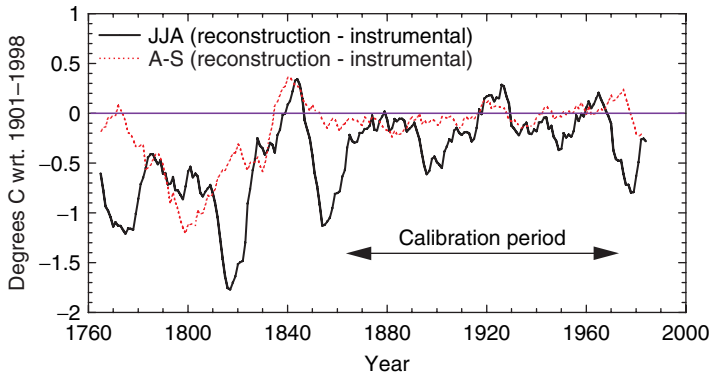


Figure 7. Anomalies (reconstructed minus instrumental) between the reconstructed and extended instrumental data from a single grid point (47 °N, 9 °E) after smoothing with an 11-year moving average, shown for both JJA (solid) and A–S (dashed). This figure is available in colour online at www.interscience.wiley.com/ijoc

 

1992; Jacoby *et al*., 1996), has been a controversial contention (Jacoby *et al*., 1996) and remains controversial as a reason (Esper *et al*., 2002; Mann and Jones, 2003) for differences in large-scale reconstructions that utilize only temperature sensitive tree-ring data or combine tree-ring and other proxy data.

Figure 8a shows the full length of the low elevation grid data for the JJA and annual seasons smoothed with an 11-year running average. A notable feature is the divergence in these records back in time, with cooler season temperatures showing a greater positive trend to the modern period than the warmer season temperatures (Böhm *et al*., 2001). In addition to these data, other long series from Europe (Luterbacher *et al*., 2004) and the northern hemisphere (Hansen *et al*., 1999; Jones *et al*., 2003) have been shown to similarly diverge. In Figure 8B, anomalies between the JJA reconstruction and the JJA instrumental (the same as from Figure 7) and anomalies between the JJA reconstruction and annual data are shown. The annual season anomalies result in smaller differences, centered more about the zero line, than the JJA data. A notable exception occurs around 1815, where both JJA and annual temperatures have essentially the same cold anomaly and hence about the same difference to the JJA reconstruction.

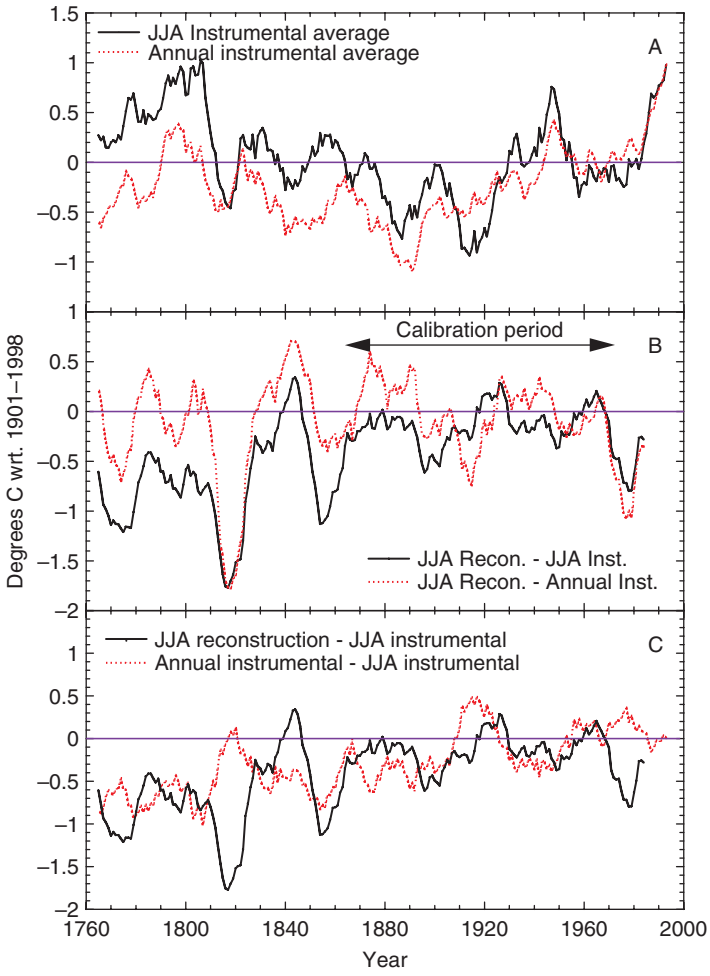


Figure 8. (A) Plot of JJA and annual 11-year smoothed instrumental data from the 47 °N, 9 °E grid point (Böhm *et al*., 2001). (B) Anomalies from reconstructed JJA temperatures, based on the ring-width data, and JJA (same as in Figure 7; solid) and annual (dashed) instrumental data. Differences between the JJA reconstruction and JJA instrumental data (solid) and the annual and JJA instrumental (dashed) are shown in (C). This figure is available in colour online at www.interscience.wiley.com/ijoc

 

Also significant is the divergence around the 1850s noted above, during which the trees reconstruct cooler conditions than the early JJA instrumental data. The latter are slightly above the twentieth-century mean, while annual temperatures for this same period are about 0.7 °C below the twentieth-century mean. This observation could be seen as additional evidence for the trees being sensitive to conditions outside the growing season on decadal timescales. For comparison, the difference between JJA and annual temperatures and the JJA reconstruction and JJA temperatures (Figure 8C) show similar patterns (except for around 1815) and a divergence of a similar rate and magnitude, a further indication for the plausibility that the trees carry more of an annual signal, in the lower-frequency domain.

It is unclear whether the situation around the turn of the nineteenth century is analogous to the 'reduced sensitivity' of trees in recent decades (Briffa *et al*., 1998) where underestimations of recent temperatures are particular evident with the maximum latewood density data. Further, the late 18th and early nineteenth centuries are also interesting in terms of homogenization of the instrumental records. Over 1.0 °C increase was added to the A–S temperature average in the correction and homogenization procedure for the Switzerland subset of climatic data during this time period (Böhm *et al*., 2001). It seems plausible that the relatively cool conditions in the early nineteenth century, preceded by warm conditions, makes it difficult to properly homogenize early instrumental data. These early instrumental data are in a 'state of motion', which is particularly critical if systematic biases are found (e.g. Chenoweth, 1993; Moberg *et al*., 2003; Jones and Lister, 2004).

Similar discrepancies were described by Esper *et al*. (2005) for large-scale reconstructions. In general, the warm season large-scale early instrumental data contains relatively warmer anomalies than the annual data, and that low-frequency trends of the proxy reconstructions themselves tend to 'undershoot' these higher anomalies.

The differences between the seasonal trends in the instrumental data, and how well the reconstructions fit these data, cannot ultimately be used to determine the exact relationship between the tree- and instrumental data in the lowest frequency domains. Trends in the tree-ring reconstructions seem to more closely match those of the annual instrumental data and 'undershoot' the summer temperature data. This occurs even though these tree-ring data, as processed here, are inherently limited in the lowest frequency domains. Age-related standardization approaches tend to 'undershoot' the early instrumental data even more (Büntgen *et al*., 2005). Noise and uncertainties in the reconstructions, and additional possibilities such as trees responding more to maximum temperatures (Wilson and Luckman, 2003), trends or changes in growing season length, precipitation changes, slow ecological shifts or even anthropogenic influences should also not be discounted.

## 6. SUMMARY

We have presented two new reconstructions for the Central and Western Alps based on a multitude of high-elevation tree-ring data. The reconstructions draw information for sites of all species across the Alpine arc as evidenced by the beta weights. Additionally, following Meko (1997) we have tested and shown improved verification statistics for a reconstruction approach using the single maximum latewood density series as predictors for PCA regression. Comparisons with extended instrumental records from the region have shown similarities in the higher frequency domain, yet some differences in the low-frequency domains remain. It is possible that these differences are the result of noise in the reconstructions, reflect more of an annual signal in the tree-ring data or long-term homogeneity issues with the instrumental data, or a combination thereof. The reconstructions will additionally allow for comparisons with recently published high-resolution gridded reconstructions based primarily on early instrumental and historical proxy data (Casty *et al*., in press), to more fully understand and address the climate history in this region, especially related to multi-decadal trends. The network will also allow for comparisons with millennial-length tree-ring data, where centennial trends in the tree-ring data have been preserved using age-related detrending methods of millennial length composite records (e.g. Büntgen *et al*., 2005).

 

ACKNOWLEDGEMENTS

We thank P. Bebi, W. Elling, H. Fritts, W. Hüsken, F. Meyer, B. Neuwirth, R. Niederer, C. Rolland, F. Schweingruber, F. Serre, L. Tessier and K. Treydte for tree-ring data obtained directly or through the ITRDB, and R. Böhro for meteorological data and R. Wilson, E. Cook, U. Büntgen, K. Treydte, F. Schweingruber and an anonymous reviewer for comments and discussions. This work was supported by the European Union Project ALP-1MP (BBW 01.0498-1) and the Swiss National Science Foundation (NCCR-VITA).

## APPENDIX I. SPLIT PERIOD CALIBRATION AND VERIFICATION STATISTICS FOR THE NESTED MODELS

A. Ring-width nests and JJA

| Model | $R^2$(Calib.)[1] | $R^2$(Verif.)[2] | RE[3] | CE[4] | PM[5] | SIGN[6] |
|---|---|---|---|---|---|---|
| 1850–1990 | 0.56/0.58 | 0.25/0.37 | 0.12/0.04 | −0.38/−0.51 | –/*** | ***/– |
| 1850–1973 | 0.64/0.68 | 0.43/0.30 | 0.36/0.37 | −0.01/0.00 | ***/*** | **/*** |
| 1800–1973 | 0.64/0.65 | 0.35/0.26 | 0.18/0.13 | −0.30/−0.37 | **/** | ***/* |
| 1750–1973 | 0.56/0.47 | 0.29/0.40 | 0.30/0.19 | −0.10/−0.28 | **/*** | ***/** |
| 1700–1973 | 0.46/0.43 | 0.27/0.34 | 0.39/0.23 | 0.04/−0.22 | ***/** | */* |
| 1650–1973 | 0.31/0.41 | 0.39/0.31 | 0.16/0.02 | −0.32/−0.55 | ***/*** | –/– |
| 1600–1973 | 0.31/0.38 | 0.39/0.26 | 0.16/0.05 | −0.32/−0.50 | ***/** | –/– |

B. Density Chronology Nests and A–S

| Model | $R^2$(Calib.)[1] | $R^2$(Verif.)[2] | RE[3] | CE[4] | PM[5] | SIGN[6] |
|---|---|---|---|---|---|---|
| 1830–1988 | 0.33/0.45 | 0.44/0.32 | 0.35/0.25 | 0.02/−0.13 | ***/*** | –/** |
| 1830–1973 | 0.43/0.54 | 0.41/0.37 | 0.31/0.29 | −0.05/−0.07 | ***/*** | –/** |
| 1780–1973 | 0.33/0.53 | 0.53/0.33 | 0.26/0.12 | −0.11/−0.33 | ***/*** | –/** |
| 1730–1973 | 0.34/0.49 | 0.49/0.34 | 0.27/0.21 | −0.11/−0.20 | ***/*** | –/** |

C. Density Individual Series Nests and A–S

| Model | $R^2$(Calib.)[1] | $R^2$(Verif.)[2] | RE[3] | CE[4] | PM[5] | SIGN[6] |
|---|---|---|---|---|---|---|
| 1850–1988 | 0.72/0.60 | 0.35/0.31 | 0.48/0.30 | 0.22/−0.06 | ***/*** | –/** |
| 1850–1973 | 0.89/0.93 | 0.56/0.40 | 0.69/0.50 | 0.54/0.24 | ***/*** | ***/*** |
| 1800–1973 | 0.73/0.84 | 0.54/0.44 | 0.64/0.61 | 0.46/0.41 | ***/*** | **/*** |
| 1750–1973 | 0.60/0.72 | 0.56/0.21 | 0.62/0.42 | 0.43/0.12 | ***/– | **/*** |
| 1700–1973 | 0.50/0.54 | 0.44/0.26 | 0.43/0.12 | 0.13/−0.33 | ***/*** | –/– |
| 1650–1973 | 0.46/0.50 | 0.40/0.26 | 0.24/0.24 | −0.15/−0.15 | ***/*** | –/** |

Calibration and verification statistics for the nested temperature models for the early/late verification periods (1864–1918/1919–1972).[1&2] Squared Pearson correlation during the calibration and verification periods.[3&4] Reduction of Error and Coefficient of Efficiency statistics-have a range from minus infinity to 1, with positive values indicating predictive skill.[5&6] Product Mean and Sign tests with significance at the 90, 95 and 99% levels denoted by one, two or three asteriskes, respectively.

 

## APPENDIX II. FULL PERIOD CALIBRATION AND EXTRA VERIFICATION STATISTICS

A. Ring-width and JJA

| Model | Number of Crnls.[a] | Number of Pred. Passed[b] | $R^2$(Calib.)[1] | $R^2$(Verif.)[2] | RE[3] | CE[4] | PM[5] | SIGN[6] |
|---|---|---|---|---|---|---|---|---|
| 1850–1990 | 21 | 21 | 0.46 | 0.49 | 0.27 | −0.03 | *** | ** |
| 1850–1973 | 45 | 50 | 0.62 | 0.39 | −0.32 | −0.87 | ** | – |
| 1800–1973 | 28 | 32 | 0.55 | 0.41 | 0.22 | 0.05 | *** | ** |
| 1750–1973 | 16 | 17 | 0.49 | 0.40 | 0.21 | −0.15 | *** | ** |
| 1700–1973 | 7 | 8 | 0.44 | 0.30 | −0.03 | −0.50 | *** | * |
| 1650–1973 | 5 | 5 | 0.31 | 0.17 | −0.08 | −0.569 | *** | – |
| 1600–1973 | 4 | 4 | 0.28 | 0.14 | −0.07 | −0.556 | *** | – |

B. Density Chronology and A–S

| Model | Number of Crnls.[a] | Number of Pred. Passed[b] | $R^2$(Calib.)[1] | $R^2$(Verif.)[2] | RE[3] | CE[4] | PM[5] | SIGN[6] |
|---|---|---|---|---|---|---|---|---|
| 1830–1988 | 5 | 6 | 0.40 | 0.51 | 0.38 | 0.34 | *** | *** |
| 1830–1973 | 19 | 22 | 0.43 | 0.57 | 0.49 | 0.47 | *** | ** |
| 1780–1973 | 7 | 10 | 0.38 | 0.45 | 0.20 | −0.10 | *** | – |
| 1730–1973 | 4 | 5 | 0.41 | 0.43 | 0.18 | −0.12 | *** | * |

C. Density Individual Series and A–S

| Model | Number of Series[a] | Number of Pred. Passed[b] | $R^2$(Calib.)[1] | $R^2$(Verif.)[2] | RE[3] | CE[4] | PM[5] | SIGN[6] |
|---|---|---|---|---|---|---|---|---|
| 1850–1988 | 97 | 121 | 0.65 | 0.41 | 0.39 | 0.32 | *** | * |
| 1850–1973 | 341 | 396 | 0.86 | 0.65 | 0.65 | 0.63 | ** | * |
| 1800–1973 | 162 | 201 | 0.74 | 0.37 | 0.34 | 0.21 | *** | *** |
| 1750–1973 | 77 | 91 | 0.67 | 0.49 | 0.27 | 0.01 | *** | *** |
| 1700–1973 | 29 | 36 | 0.52 | 0.41 | 0.13 | −0.20 | *** | ** |
| 1650–1973 | 12 | 17 | 0.45 | 0.42 | 0.17 | −0.14 | *** | ** |

Statistics for the nested temperature models for the full (1864–1972) calibration period. [a&b] Number of series available for each time period and the total number of predictors that passed correlation screening and entered into the principal components analysis. The maximum number of predictors is twice the number of chronologies.[1–6] As in Appendix I, except using the maximum overlap with the low-elevation early instrumental data from 1760–1863. See text for details. For the first nest in each reconstruction, with more recent data than the 1972 end of the calibration period, the high elevation data from 1973–1989 and from 1973–1987 were also used to compute the verification statistics for the ring-width and density reconstructions, respectively.

### REFERENCES

Akaike H. 1974. A new look at the statistical model identification. *IEEE Transactions on Automatic Control* **19**: 716–723.

Auer I, Böhm R, Maugeri M. 2000. A new long-term gridded precipitation data-set for the Alps and its application for map and alpclim. *Journal for Physics and Chemistry of the Earth*, Part B, **26**: 421–424.

Böhm R, Auer I, Brunetti M, Maugeri M, Nanni T, Schöner W. 2001. Regional temperature variability in the European Alps 1760–1998 from homogenized instrumental time series. *International Journal of Climatology* **21**: 1779–1801.

Briffa KR. 2000. Annual climate variability in the Holocene: interpreting the message of ancient trees. *Quaternary Science Reviews* **19**: 87–105.

Briffa KR, Jones PD, Schweingruber FH. 1988. Summer temperature patterns over Europe: a reconstruction from 1750 A.D. based on maximum latewood density indices of conifers. *Quaternary Research* **30**: 36–52.

Briffa KR, Schweingruber FH, Jones PD, Osborn TJ, Shiyatov SG, Vaganov EA. 1998. Reduced sensitivity of recent tree-growth to temperature at high northern latitudes. *Nature* **391**: 678–682.

Briffa KR, Osborn TJ, Schweingruber FH, Jones PD, Shiyatov SG, Vaganov EA. 2002a. Tree-ring width and density data around the Northern Hemisphere: part 1, local and regional climate signals. *The Holocene* **12**: 737–757.

 

Briffa KR, Osborn TJ, Schweingruber FH, Jones PD, Shiyatov SG, Vaganov EA. 2002b. Tree-ring width and density data around the Northern Hemisphere: Part 2, spatio-temporal variability and associated climate patterns. *The Holocene* **12**: 759–789.

Briffa KR, Osborn TJ, Schweingruber FH, Harris IC, Jones PD, Shiyatov SG, Vaganov EA. 2001. Low-frequency temperature variations from a northern tree ring density network. *Journal of Geophysical Research* **106**: 2929–2941.

Briffa KR, Jones PD, Bartholin TS, Eckstein D, Schweingruber FH, Karlén W, Zetterberg P, Eronen M. 1992. Fennoscandian summers from AD 500: temperature changes on short and long timescales. *Climate Dynamics* **7**: 111–119.

Büntgen U, Esper J, Frank DC, Nicolussi K, Schmidhalter M. 2005. A 1052-year tree-ring proxy for Alpine summer temperatures. *Climate Dynamics*. DOI: 10.1007/s00382-005-0028-1

Casty C, Luterbacher J, Wanner H, Esper J,Böhm R. In press. Temperature and precipitation variability in the European Alps since 1500. *International Journal of Climatology*.

Chenoweth M. 1993. Nonstandard thermometer exposures at U.S. cooperative weather stations during the late nineteenth century. *Journal of Climate* **6**: 1787–1797.

Cook ER. 1985. *A time series analysis approach to tree-ring standardization*. PhD dissertation, University of Arizona, Tucson, AZ.

Cook ER, Peters K. 1981. The smoothing spline: a new approach to standardizing forest interior tree-ring width series for dendroclimatic studies. *Tree-Ring Bulletin* **41**: 45–53.

Cook ER, Peters K. 1997. Calculating unbiased tree-ring indices for the study of climatic and environmental change. *The Holocene* **7**: 361–370.

Cook ER, Briffa KR, Jones PD. 1994. Spatial regression methods in dendroclimatology: a review and comparison of two techniques. *International Journal of Climatology* **14**: 379–402.

Cook ER, D'Arrigo RD, Mann ME. 2002. A well-verified, multiproxy reconstruction of the winter North Atlantic Oscillation index since A.D. 1400. *Journal of Climate* **15**: 1754–1764.

Cook ER, Krusic PJ, Jones PD. 2003. Dendroclimatic signals in long tree-ring chronologies from the Himalayas of Nepal. *International Journal of Climatology* **23**: 707–732.

Cook ER, Esper J, D'Arrigo R. 2004. Extra-tropical Northern Hemisphere temperature variability over the past 1000 years. *Quaternary Science Reviews* **23**: 2063–2074.

Cook ER, Briffa KR, Meko DM, Graybill DS, Funkhouser G. 1995. The 'segment length curse' in long tree-ring chronology development for paleoclimatic studies. *The Holocene* **5**: 229–237.

Crowley TJ. 2000. Causes of climate change over the past 1000 years. *Science* **289**: 270–277.

D'Arrigo RD, Jacoby GC, Free R. 1992. Tree ring-width and maximum latewood density at the North American tree line: parameters of climatic change. *Canadian Journal of Forest Research* **22**: 1290–1296.

Esper J, Cook ER, Schweingruber FH. 2002. Low-frequency signals in long tree-ring chronologies for reconstructing of past temperature variability. *Science* **295**: 2250–2253.

Esper J, Frank DC, Wilson RJS. 2004. Climate reconstructions: low-frequency ambition and high-frequency ratification. *Earth Observing System* **85**: 133,120.

Esper J, Frank DC, Wilson RJS, Briffa KR. 2005. Effect of scaling and regression on reconstructed temperature amplitude for the past millennium. *Geophysical Research Letters* **32**: DOI.1029/2004GL021236

Esper J, Shiyatov SG, Mazepa VS, Wilson RJS, Graybill DA, Funkhouser G. 2003. Temperature-sensitive Tien Shan tree ring chronologies show multi-centennial growth trends. *Climate Dynamics* **8**: 699–706.

Frank DC, Esper J. 2005. Characterization and climate response patterns of a high elevation, multi species tree-ring network in the European Alps. *Dendrochronologia* **22**: 107–121.

Hansen J, Ruedy R, Glascoe J, Sato M. 1999. GISS analysis of surface temperature change. *Journal of Geophysical Research* **104**: 30 997–31 022.

Jacoby GC, D'Arrigo R. 1989. Reconstructed northern hemisphere annual temperature since 1671 based on high-latitude tree-ring data from North America. *Climatic Change* **14**: 39–59.

Jacoby G, D'Arrigo R, Luckman B. 1996. Millennial and near-millennial scale dendroclimatic studies in northern North America. In *Climatic Variations and Forcing Mechanisms of the Last 2000 Years*, *NATO ASI Series, Vol. I41*, Jones PD, Bradley RS, Jouzel J (eds). Springer-Verlag: Berlin; 67–84.

Jones PD, Lister D. 2004. The development of monthly temperature series for Scotland and Northern Ireland. *International Journal of Climatology* **24**: 569–590. DOI: 10.1002/joc.1017

Jones PD, Osborn TJ, Briffa KR. 2003. Changes in the Northern Hemisphere annual cycle: implications for paleoclimatology? *Journal of Geophysical Research* **108**: 4588. DOI:10.1029/2003JD003695

Jones PD, Briffa KR, Barnett TP, Tett SFB. 1998. High-resolution palaeoclimatic records for the past millennium-interpretation, integration and comparison with general circulation model control-run temperatures. *The Holocene* **8**: 455–471.

Luterbacher J, Dietrich D, Xoplaki E, Grosjean M, Wanner H. 2004. European seasonal and annual temperature variability, trends and extremes since 1500 A.D. *Science* **303**: 1499–1503.

Luterbacher J, Xoplaki E, Dietrich D, Rickli R, Jacobeit J, Beck C, Gyalistras D, Schmutz C, Wanner H. 2002. Reconstruction of sea level pressure fields over the eastern North Atlantic and Europe back to 1500. *Climate Dynamics* **18**: 545–561. DOI: 10.1007/s00382-001-0196-6

Mann ME, Jones PD. 2003. Global surface temperatures over the past two millennia. *Geophysical Research Letters* **30**: DOI: 10.1029/2003GL017814

Mann ME, Bradley RS, Hughes MK. 1999. Northern Hemisphere temperatures during the past millennium: inferences, uncertainties, and limitations. *Geophysical Research Letters* **26**: 759–762.

Meko DM. 1997. Dendroclimatic reconstruction with time varying predictor subsets of tree indices. *Journal of Climate* **10**: 687–696.

Meko DM, Therrell MD, Baisan CH, Hughes MK. 2001. Sacramento River flow reconstructed to AD 869 from tree rings. *Journal of the American Water Resources Association* **37**: 1029–1039.

Moberg A, Alexandersson H, Bergström H, Jones PD. 2003. Were southern Swedish summer temperatures before 1860 as warm as measured? *International Journal of Climatology* **23**: 1495–1521.

 

Moberg A, Sonechkin DM, Holmgren K, Datsenko NM, Karlén W. 2005. Highly variable Northern Hemisphere temperatures reconstructed from low- and high-resolution proxy data. *Nature* **433**: 613–617.
Nicolussi K, Schiessling P. 2001. Establishing a multi-millenial *Pinus cembra* chronology for the central Eastern Alps. In *International Conference of Tree-Rings and People*, Kaennel Dobbertin M, Bräker OU (eds). Davos, 22–26 September 2001. Abstracts. Swiss Federal Research Institute WSL, Birmensdorf. 87.
Osborn TJ, Briffa KR, Jones PD. 1997. Adjusting variance for sample-size in tree-ring chronologies and other regional-mean time-series. *Dendrochronologia* **15**: 89–99.
Peters K, Jacoby GC, Cook ER. 1981. Principal components analysis of tree-ring sites. *Tree-Ring Bulletin* **41**: 1–19.
Pfister C. 1999. *Wetternachhersage: 500 jahre klimvariationen und naturkatastrophen (1496–1995)*. Haupt: Bern.
Schweingruber FH, Briffa KR. 1996. Tree-ring density networks for climate reconstruction. In *Climatic Variations and Forcing Mechanisms of the Last 2000 Years*, *NATO ASI Series, Vol. I41*, Jones PD, Bradley RS, Jouzel J (eds). Springer-Verlag: Berlin; 43–66.
Schweingruber FH, Bräker OU, Schär E. 1987. Temperature information from a European dendroclimatological sampling network. *Dendrochronologia* **5**: 9–33.
Serre-Bachet F, Martinelli N, Pignatelli O, Guiot J, Tessier L. 1991. Evolution des temperatures du Nord-Est de l'Italie depuis 1500 A.D. reconstruction d'apres les cernes des arbres. *Dendrochronologia* **9**: 213–229.
Wanner H, Rickli R, Salvisberg E, Schmutz C, Schüepp M. 1997. Global climate change and variability and its influence on alpine climate-concepts and observations. *Theoretical and Applied Climatology* **58**: 221–243.
Weisberg S. 1985. *Applied Linear Regression*, 2nd edn. John Wiley: New York.
Wilson RJS, Luckman BH. 2003. Dendroclimatic reconstruction of maximum summer temperatures from upper treeline sites in Interior British Columbia, Canada. *The Holocene* **13**: 851–861.
Wilson RJS, Topham J. 2004. Violins and climate. *Theoretical and Applied Climatology* **77**: 9–24.

 